Title

Predictive Value of Deep Learning-derived CT Pectoralis Muscle and Adipose Measurements for Incident Heart Failure: Multi-Ethnic Study of Atherosclerosis.

Journal

Radiology: Cardiothoracic Imaging, 5(5)

Authors

Hathaway, Quincy
Ibad, Hamza
Bluemke, David
et al.

Publication Date

2023-10-01

DOI

10.1148/ryct.230146

Peer reviewed

Radiology: Cardiothoracic Imaging

Predictive Value of Deep Learning–derived CT Pectoralis Muscle and Adipose Measurements for Incident Heart Failure:

Multi-Ethnic Study of Atherosclerosis

Quincy Hathaway*

Hamza Ahmed Ibad*

David A. Bluemke

Farhad Pishgar

Arta Kasaiean

Joshua G. Klein

Rebecca Cogswell

Matthew Allison

Matthew J. Budoff

R. Graham Barr

Wendy Post

Miriam A. Bredella

João A. C. Lima

Shadpour Demehri, MD

From the School of Medicine, West Virginia University, Morgantown, WV (Q.H.); Russell H. Morgan Department of Radiology and Radiological Sciences (H.A.I., F.P., A.K., J.G.K., S.D.) and Division of Cardiology, Department of Medicine (W.P., J.A.C.L.), Johns Hopkins University School of Medicine, 601 N Caroline St, JHOC 5165, Baltimore, MD 21287; Department of Radiology, University of Wisconsin School of Medicine and Public Health, Madison, Wis (D.A.B.); Department of Medicine, University of Minnesota, Minneapolis, Minn (R.C.); Department of Family Medicine and Public Health, University of California San Diego, La Jolla, Calif (M.A.); Lundquist Institute at Harbor-University of California Los Angeles School of Medicine, Torrance, Calif (M.J.B.); Departments of Medicine and Epidemiology, Columbia University Medical Center, New York, NY (R.G.B.); and Department of Radiology, Massachusetts General Hospital and Harvard Medical School, Boston, Mass (M.A.B.). Received XXX; revision requested XXX; revision received XXX; accepted XXX. Supported by the National Heart, Lung, and Blood Institute (grants 75N92020D00001, HHSN268201500003I, N01-HC-95159, 75N92020D00005, N01-HC-95160, 75N92020D00002, N01-HC-95161, 75N92020D00003, N01-HC-95162, 75N92020D00006, N01-HC-95163, 75N92020D00004, N01-HC-95164, 75N92020D00007, N01-HC-95165, N01-HC-95166,

N01-HC-95167, N01-HC-95168, N01-HC-95169, R01-HL-077612, and R01-HL-093081), the National Center for Advancing Translational Sciences (grants UL1-TR-000040, UL1-TR-001079, and UL1-TR-001420) and the NIH National Institute of Arthritis and Musculoskeletal and Skin Diseases (grant R01AR079620). This publication was developed under a STAR research assistance agreement, no. RD831697 (MESA Air) and RD-83830001 (MESA Air Next Stage), awarded by the U.S. Environmental Protection Agency (EPA). It has not been formally reviewed by the EPA. The views expressed in this document are solely those of the authors and the EPA does not endorse any products or commercial services mentioned in this publication. The information contained herein was derived in part from data provided by the Bureau of Vital Statistics, New York City Department of Health and Mental Hygiene. **Address correspondence to** S.D. (email: *Demehri2001@yahoo.com*).

* Q.H. and H.A.I. contributed equally to this work.

https://doi.org/10.1148/ryct.230146

Purpose: To develop a deep learning algorithm capable of extracting pectoralis muscle and adipose measurements and to longitudinally investigate associations between these measurements and incident heart failure (HF) in participants from the Multi-Ethnic Study of Atherosclerosis (MESA).

Materials and Methods: MESA is a prospective study of subclinical cardiovascular disease characteristics and risk factors for progression to clinically overt disease approved by institutional review boards of six participating centers (ClinicalTrials.gov identifier: NCT00005487). All participants with adequate imaging and clinical data from the fifth examination of MESA were included in this study. Hence, in this secondary analysis, manual segmentations of 600 chest CT examinations (between the years 2010 and 2012) were used to train and validate a convolutional neural network, which subsequently extracted pectoralis muscle and adipose (intermuscular adipose tissue (IMAT), perimuscular adipose tissue (PAT), extramyocellular lipids and subcutaneous adipose tissue) area measurements from 3031 CT examinations using individualized thresholds for adipose segmentation. Next, 1781 participants without baseline HF were longitudinally investigated for associations between baseline pectoralis muscle and adipose measurements and incident HF using crude and adjusted Cox proportional hazards models. The full models were adjusted for variables in categories of demographic (age, race, sex, income), clinical/laboratory (including physical activity, BMI, and smoking), CT (coronary artery calcium score), and cardiac MRI (left ventricular ejection fraction and mass (% of predicted)) data.

Results: In 1781 participants (median age, 68 (IQR,61, 75) years; 907 [51%] females), 41 incident HF events occurred over a median 6.5-year follow-up. IMAT predicted incident HF in unadjusted (hazard ratio [HR]:1.14; 95%CI: 1.03–1.26) and fully adjusted (HR:1.16, 95%CI: 1.03–1.31) models. PAT also predicted incident HF in crude (HR:1.19; 95%CI: 1.06–1.35) and fully adjusted (HR:1.25; 95%CI: 1.07–1.46) models.

Conclusion: The study demonstrates that fast and reliable deep learning-derived pectoralis muscle and adipose measurements are obtainable from conventional chest CT, which may be predictive of incident HF.

Although causal inference cannot be established in this observational study, longitudinal associations were found between potentially modifiable CT-based pectoralis measurements and incident heart failure after adjustment for clinical and imaging confounders.

Abbreviations
EML = Extramyocellular Lipids, HF = Heart Failure, IMAT = Intermuscular Adipose Tissue, MESA = Multi-Ethnic Study of Atherosclerosis, PAT = Perimuscular Adipose Tissue, PMT = Pectoralis Muscle Tissue, SAT = Subcutaneous Adipose Tissue

Key Points

A deep-learning algorithm for pectoralis muscle and adipose area measurements was developed using individualized thresholds from 3031 chest CT examinations in participants from the Multi-Ethnic Study of Atherosclerosis (Dice scores: 0.90 for training/testing sets).

Models were adjusted for a comprehensive set of confounders, including physical activity, left ventricular ejection fraction and mass (% of predicted), and coronary artery calcium score.

In fully adjusted models in 1781 participants without baseline heart failure, intermuscular (hazard ratio:1.16, 95% CI: 1.03, 1.31) and perimuscular adipose tissue (hazard ratio:1.25, 95% CI: 1.07, 1.46) predicted incident heart failure (n = 41 events).

Author contributions:
Guarantor of integrity of entire study, **Q.H., S.D.**; study concepts/study design or data acquisition or data analysis/interpretation, all authors; manuscript drafting or manuscript revision for important intellectual content, all authors; approval of final version of submitted manuscript, all authors; agrees to ensure any questions related to the work are appropriately resolved, all authors; literature research, **Q.H., H.A.I., F.P., J.G.K., M.J.B., M.A.B., J.A.C.L., S.D.**; clinical studies, **D.A.B., F.P., A.K., J.G.K., M.A., M.J.B., R.G.B., S.D.**; experimental studies, **Q.H.**; statistical analysis, **Q.H., H.A.I.**; and manuscript editing, **Q.H., H.A.I., D.A.B., F.P., J.G.K., R.C., M.A., M.J.B., W.P., M.A.B., J.A.C.L., S.D.**

Conflicts of interest are listed at the end of this article.

Heart failure (HF) incidence rates are increasing, with an estimated annual incidence of one million patients in the United States and currently affecting ~ 26 million patients worldwide (1,2).

Study of risk factors for the prediction of HF has become a rapidly emerging focus of clinical interest to mitigate these rising trends (3–5). However, compared with prediction models of other cardiovascular diseases (eg, Framingham Risk score for coronary heart disease) (6), HF incidence prediction models are relatively new (7,8) and perhaps less robust than models predicting HF-related hospitalization or mortality (9–12). Variables traditionally identified as risk factors for HF or HF-related outcomes include demographic factors (13), clinical factors (eg, physical activity, hypertension, and diabetes) (3), and imaging biomarkers (eg, Agatston score (14) and MRI-derived left ventricular mass (15) and ejection fraction (9)).

Therefore, identifying and validating other potentially “modifiable” factors (eg, muscle loss) that can predict incident HF independent of traditionally predictive clinical and imaging

biomarkers can be pivotal to implement secondary preventative measures (eg, adequate nutrition and physical rehabilitation to mitigate muscle loss) in at-risk populations (16–18). Future studies may also investigate the role of these CT-derived markers to monitor the effect of these secondary preventive measures. Additionally, identification of at-risk individuals may also lower the threshold of clinical suspicion, which can improve HF-related outcomes and thereby prevent hospitalizations and mortality.

One established morbidity in the setting of advanced HF is "cardiac cachexia," defined as unintentional lean body mass loss concurrent with advanced cardiac dysfunction (16). Cardiac cachexia is a relatively well-established condition with prior studies associating cachexia and HF either through cross-sectional analyses or longitudinal observations in patients with pre-existing HF (19,20). Studies have shown that nutritional support (16,18,21) as well as physical rehabilitation (16,21) may improve cardiac cachexia, which further justify the investigation of the associated biomarkers for muscle loss as modifiable predictors for HF incidence.

A recent study demonstrated an association between CT-based adipose tissue measurements in thigh muscles and HF (22). Compared with thigh muscle groups, pectoralis muscles are opportunistically imaged in any conventional chest CT examination (eg, during CT for Agatston score) and can provide opportunities to improve HF incidence prediction model performances at no additional cost or radiation.

Previously, CT-based muscle measurements have been limited to research settings due to the time-consuming and complex nature of manual postprocessing techniques. With recent advances in deep learning algorithms, fast and reliable muscle measurements are now feasible (23). These advances may facilitate their implementation into routine clinical practice. CT-based pectoralis muscle measurements have previously been shown to have predictive value for other health outcomes, such as all-cause mortality in patients with chronic obstructive pulmonary disease (24) and COVID-19 (25).

The present study aims to develop a deep learning algorithm capable of fast and reliable pectoralis muscle and adipose area (in cm^2) measurements, including intermuscular adipose tissue (IMAT), perimuscular adipose tissue (PAT), extramyocellular lipids (EML) and subcutaneous adipose tissue (SAT) measurements, and to longitudinally investigate associations between these measurements and incident HF in the Multi-Ethnic Study of Atherosclerosis (MESA; https://www.mesa-nhlbi.org).

Materials and Methods

MESA is a prospective study designed to investigate subclinical cardiovascular disease characteristics and risk factors for progression to clinical manifestation. At baseline (2000–2002), MESA enrolled 6,814 individuals aged 45–84 years from various racial backgrounds. Eligibility was determined based on age and geographic boundaries for each field center. Participants with known clinical cardiovascular disease were excluded. Thus, participants with and without subclinical cardiovascular disease were recruited (26). The study is approved by the institutional review boards of its six participating field centers (Columbia University, Johns Hopkins University, Northwestern University, University of California, University of Minnesota,

and Wake Forest University) and its coordinating center (University of Washington) (ClinicalTrials.gov identifier: NCT00005487) and is compliant with the Health Insurance Portability and Accountability Act. Participants provided written informed consent at enrollment (24).

In MESA's fifth examination (conducted April 2010–January 2012), 3137 participants underwent noncontrast chest CT (distinct from CT scans performed for Agatston score) for the MESA Lung ancillary study. The current analysis includes participants (n = 3083) from the MESArthritis ancillary study (which uses participant data from the main MESA's fifth examination (2010–2012) as its baseline data), which is a subancillary study of participants from the MESA Lung ancillary study (Fig 1) (24).

Imaging Biomarkers

Coronary artery calcium CT scans.—

Cardiac-gated electron-beam CT or multidetector CT (Imatron C150, LightSpeed QXi, LightSpeed Plus; GE Medical Systems, Milwaukee, Wis; Volume Zoom, Siemens, Erlangen, Germany; voltage, 120–140 kVp; rotation time, 0.5–0.8 seconds; effective current: 630mA or body weight dependent; reconstructed field of view: 350 m) were used to calculate the Agatston score between 2010–2012. Two consecutive scans were obtained and independently analyzed for coronary artery plaque calcifications. An in-house software was used for Agatston score measurement (27,28).

MRI-derived left ventricular mass.—

1.5 Tesla MRI examinations (Avanto and Espree, Siemens Medical Systems; and Signa HD, GE Healthcare) were used to assess left ventricular mass and volumes between 2010–2012. A cine fast gradient-echo sequence with temporal resolution ≤ 40 msec acquired short-axis images over the left ventricle. Left ventricular mass (% of Predicted) was calculated as follows:

$$100 * \frac{\left(\text{End - Diastolic Myocardial Area * Section Thickness}\right) + \left(\text{Intersection gap * Myocardial Specific Gravity (1.05 g / ml)}\right)}{\text{a} * \text{height} \wedge 0.54 * \text{weight} \wedge 0.61}$$

(5)(5). A publicly accessible calculator is available at https://www.mesa-nhlbi.org/MESALVmass/MesaLVMPercentPredicted.aspx (5).

Chest CT scans.—

In addition to CAC CT scans, a 64-section multidetector row CT scanner (LightSpeed and Discovery, GE Healthcare; Somatom Sensation and Somatom Definition, Siemens Medical Solutions) was used to perform noncontrast chest CT examinations between 2010–2012, following the MESA Lung and Subpopulations and Intermediate Outcomes in COPD Study Protocol (voltage: 120 kVp; pitch: 0.984; rotation time: 0.500 seconds; effective current setting was based on the participants' body mass index). Monthly lung phantom calibrations were performed, and examinations were reconstructed at 0.625 mm (24,29).

Deep Learning Algorithm–pectoralis Muscle and Adipose Area Measurements

Manual segmentation.—

Manual pectoralis muscle tissue (ie, pectoralis major and minor) (PMT) and SAT areas were initially measured on chest CT examinations. In 600 participants, manual measurements of PMT and SAT were performed using LabelMe (v5.1.0) (30) by two trained observers with two years of interpreting research images (Authors B and E). These observers were trained by Author N (a musculoskeletal radiologist with 15 years of experience) using 50 sample images. Labels were created for the right PMT, left PMT, and SAT. These manual traces were divided into 60% training (n = 360) and 40% hold-out (n = 240) sets (Fig 2).

DICOM to PNG conversion.—

Primary axial CT images with the thinnest slices were recursively selected using glob2 (v0.7) from the Digital Imaging and Communications in Medicine (DICOM) image list of each participant. DICOM images were windowed to a width of 250 and length of 50, converted to a 255-pixel grayscale image and saved as PNGs with OpenCV (v4.7.0.68; https://opencv.org/) (31), keeping the original resolution.

Frame selection.—

Frames directly superior to the aortic arch were selected for subsequent analysis. Our algorithm starts by removing all frames containing abdominal sections. Next, it crops the chest CT images, focusing on the mediastinum. The presentation of mediastinal structures such as the heart, pulmonary vasculature, and other venous and arterial vessels allowed for automatic selection of the frame directly superior to the aortic arch. For example, moving superiorly through the mediastinum, as the aortic arch disappears, the brachiocephalic, left common carotid, and left subclavian arteries have the lowest pixel intensities; pixel intensity increases moving superiorly as the thymus and sternum move within our cropped mediastinal view (Fig 3).

Semantic segmentation.—

Using PixelLib (dependencies: Mask region-based convolutional neural network [*R*-CNN]; labelmetococo (v0.1.2); tensorflow (v2.5.3); keras (v2.4.3)), training images were utilized to build the semantic segmentation platform, identifying the right PMT, left PMT, and SAT. Briefly, the Mask *R*-CNN algorithm (13) is a Faster *R*-CNN extension that allows for mask identification. The Mask *R*-CNN algorithm is augmented using PixelLib to allow for custom segmentation projects. We configured our transfer learning model using ResNet50 with pretrained weights (ie, common objects in context, or COCO). Following training, the algorithm was assessed on the 40% hold-out set.

The Python code was developed in Python 3.7 in Jupyter Notebook on a Dell Precisions Workstation T5810 with 256 GB RAM. The operating system was native Linux, Ubuntu 18.04 LTS. Further information is provided on our GitHub page (https://github.com/qahathaway/Automated_Segmentation_PTM-IMAT-SAT). Since our code is written in Python and is executable on either a central processing unit or graphics processing unit, it can theoretically be used through in-house applications or via cloud implementation.

We now include a Google Colab Jupyter Notebook that allows users to access a sample patient population (ie, patient 1, patient 2, and patient 3 in the "Example" folder under the main Github branch) and run the code to perform the following: 1) generate a single image above the aortic arch, 2) predict the semantic segmentation images, and 3) produce individual regions of interest. We have also now included the COCO pretrained weights on the GitHub page, which will allow other users to apply our developed weights on their own datasets.

Individualized threshold-based adipose tissue segmentation.—

We quantified adipose deposits existing between muscle fibers (EML) and between pectoralis major and minor (PAT), together constituting IMAT (Fig 4 and Fig E1). IMAT was isolated as previously described (32), using SAT attenuations to determine individualized thresholds. First, a histogram of SAT attenuation values was extracted. Then, we trimmed values that had a frequency < 30% as much as the mode value from both upper and lower histogram limits. The IMAT threshold was calculated as pixel values ≤ 2 standard deviations from the mean of remaining values as described by Mühlberg et al (32). Further, we separated IMAT into PAT and EML; thresholds were defined as pixel values ≤ 1 standard deviation above the mean (PAT) and between 1–2 standard deviations above the mean (EML) (Fig 4). Intramyocellular lipids can only be measured indirectly through CT muscle tissue attenuation and are considered part of PMT in this study. Total areas were calculated as the sum of bilateral pectoralis muscle and adipose area measurements. Measurements were indexed to the participants' heights.

Outcome-incident HF

Adjudication of events has been published in detail previously (5). Briefly, after the first MESA examination, participants were followed with a combination of in-person and telephonic interviews every 9–12 months to obtain hospital admission, outpatient cardiovascular disease diagnoses, and mortality data. Endpoint classification was performed by two independent physicians from the MESA study events committee using MESA study criteria. Disagreements were settled through consensus of the entire MESA study events committee. HF event criteria included probable HF events (physician diagnosis or medical treatment) or definitive HF events (diagnostic criteria of probable HF with pulmonary edema/dilated ventricle on radiography or poor left ventricular function/evidence of left ventricular diastolic dysfunction) (5). Participants were followed through 2017.

Statistical Analysis

Dice scores and intersection over union scores were calculated for training and testing sets to compare deep learning model measurements with the 600 manual tracings of PMT areas of either side and SAT area.

Kaplan-Meier estimates of incident HF for PMT, IMAT, EML, PAT, and SAT indexes (cm^2/m^2) were categorized using median values (Fig 5). Associations between PMT, SAT, PAT, EML, and IMAT indexes with incident HF in identified participants with complete data (n = 1781) were studied using several Cox proportional hazards models.

Crude Models were unadjusted for potential confounders. Fully adjusted models were adjusted for age, sex, race, income, moderate to vigorous exercise (metabolic equivalent of task-minutes/week), body mass index (BMI), pack-years of smoking, alcohol use, hypertension (JNC VI Criteria; systolic blood pressure ≥ 140 mmHg or diastolic blood pressure ≥ 90 mmHg) (33), hemoglobin A1C (%), total cholesterol (NCEP guidelines) (34), hypertension medication use, insulin/hypoglycemic medication use, lipid-lowering agent use, creatinine (mg/dL), log (Phantom Adjusted Total Agatston score), left ventricular ejection fraction and mass (% of predicted). The clinical markers used in our adjustment models have been used in prior studies for adjustment when investigating incident HF (5,22). To facilitate the interpretation of our results in clinical practice, the above models were also repeated for raw area measurements instead of indexed measurements (Table E2).

All models were tested for proportional hazards assumption using Schoenfeld residuals on time (35). Hazard ratio, 95% confidence intervals and *P* values for the pectoralis muscle and adipose measurements are reported. Harrell's C-statistics (36) and Kent and O'Quigley Pseudo-R^2 (37) are reported for each set of models.

A False Discovery Rate adjusted *P* value was used as the threshold for statistical significance for each set of models to account for the five distinct muscle measurements investigated. All analyses were performed using R (version 4.2.0; R Foundation for Statistical Computing; packages: haven, survival, dplyr, naniar, gtsummary).

Results

Participant Characteristics

Of 3083 participants with available CT scans in MESArthritis, 52 participants were excluded due to inadequate CT scans (low-quality CT (*n* = 26); breast implants (*n* = 19); artificial cardiac pacemakers (*n* = 7)), 851 were excluded due to incomplete cardiac MRI data, and 93 were excluded due to incomplete demographic, clinical, and/or laboratory data.

Subsequently, 306 participants who developed HF before their baseline MESArthritis visit (ie, fifth examination of MESA) were excluded. Hence, a total of 1,781 participants (median age, 68 [IQR, 61–75] years; 907 [51%] females, 874 [49%] males) from MESArthritis were selected for subsequent analysis (Fig 1).

Table 1 shows descriptive statistics of included individuals (*n* = 1,781). Median pack-years of smoking was found to be 0 years (IQR: 0 years-13.5 years). 53% of our sample was hypertensive, with a median hemoglobin A1C of 5.7%.

Deep Learning Model Performance

Compared with manual measurements, the Dice score of the training set was 0.90 (95% CI: 0.90–0.91), and the intersection over-union score was 0.82 (95%CI: 0.82–0.83). Similar scores were found for the testing set (Dice Score: 0.90 (95%CI: 0.89–0.90) and intersection over union score: 0.81 (95%CI: 0.81–0.82)). Individual element scores are presented in Table 2.

For a single patient, the mean time taken by the automated segmentation platform to load a DICOM series, select the primary axial frames and convert to PNG, select the single PNG directly above the aortic arch, process the image through segmentation, provide Hounsfield Unit information on the selected image, and provide measurements of all reported indexes was 2 minutes and 43 seconds. In comparison, the mean time taken by 1 observer for manual measurements of 10 randomly selected participant for all of the above processes was found to be 3 minutes and 21 seconds.

Longitudinal Associations of Pectoralis Muscle and Adipose Indices with Incident HF

A total of 41 participants developed incident HF over a median 2393 days (IQR: 2202, 2552 days) of follow-up. In crude models, higher IMAT (Hazard Ratio (HR): 1.14, 95%CI: 1.03, 1.26) and PAT (HR: 1.19, 95%CI: 1.06–1.35) indexes predicted incident HF. These associations held true after consideration of potential confounders. Higher indexes of both IMAT (HR: 1.16, 95%CI: 1.03, 1.31) and PAT (HR: 1.25, 95%CI: 1.07, 1.46) also predicted incident HF in fully adjusted models (Table 3). Repeated analyses using raw area measurements instead of indexed measurements showed similar results. HRs for IMAT and PAT were 1.05 and 1.08 in fully adjusted models, corresponding to a 5% and 8% increased risk of incident HF for every 1 cm^2 increase in IMAT and PAT, respectively (Table E2).

Harrell's C-statistics and Kent and O'Quigley Pseudo-R^2 values are reported in Table E1. Log Likelihood Ratio tests comparing models with and without pectoralis muscle and adipose indexes showed significant differences in models including IMAT (log-likelihood ratio, +2.32; P = .03) and PAT (log-likelihood ratio, +2.87; P = .02).

Discussion

In crude models and full models adjusted for clinical and imaging variables, higher CT-based IMAT and PAT indexes derived from a deep learning model were predictive of incident HF within a multiethnic cohort of participants. Analyses repeated using raw area (cm^2) measurements instead of indexed measurements revealed similar associations, with fully adjusted models conferring a 5% (IMAT) and 8% (PAT) increased chance of incident HF with every 1 cm^2 increase.

Our study is distinct from previous works in several ways (4,22). The deep learning algorithm developed for our study can potentially be implemented on any conventional chest CT examination. This is advantageous in clinical practice as chest CT examinations are often acquired in individuals at-risk for common cardiothoracic disorders (eg, Agatston score in individuals at-risk for coronary artery disease or lung cancer screening in long-time smokers) (38,39). Of > 7 million CT scans performed in the United States each year, 0.5 million are estimated to be CAC CT scans (40,41). Our findings may be especially applicable to patients with identifiable risk factors for both incident HF and coronary artery disease, including hypertension, dyslipidemia, and smoking (42).

Importantly, pectoralis muscle and adipose measurements may be derived from alternative cross-sectional imaging such as cardiac MRI. As such, these measurements may be used instead of CT-derived measurements depending on which type of scan is available. In particular, while individuals without HF may be more likely to have a chest CT acquisition (eg, CAC CT scan), individuals already diagnosed with HF may likely have cardiac MRI acquisitions for evaluation of ejection fraction, wall motion abnormalities, and microvascular obstruction (43).

In this regard, cardiac MRI-derived measurements may be used for prediction of downstream events after the initial HF diagnosis. For example, Cunha et al have shown that lower cardiac MRI-derived pectoralis muscle area measurements were an independent predictor of all-cause death or HF hospitalization in patients with HF with reduced ejection fraction (44). Similarly, Kumar et al found that a lower cardiac MRI-derived pectoralis muscle area was associated with a higher risk of mortality in patients both with and without HF, regardless of ejection fraction (45). While PMT area was not specifically found to be associated with incident HF in our study and cardiac MRI-derived pectoralis measurements of adiposity (eg, IMAT) were not studied by Cunha et al and Kumar et al, our results suggest that pectoralis muscle and adipose measurements may play an essential role in both HF incidence and downstream adverse events. Further studies may investigate the role of tissue-specific pectoralis muscle and adipose measurements at different points in the context of HF (eg, the difference in predictive value of PMT for HF incidence as opposed to its value for downstream events after an established diagnosis of HF). In particular, there is a need to investigate the utility of cardiac-MRI derived pectoralis adipose measurements (ie, IMAT, PAT, EML etc) for HF and HF-related events.

Our study demonstrates that deep learning algorithms may provide reliable muscle measurements. Deep learning algorithms can eliminate barriers like time consuming and complicated manual postprocessing and measurement techniques. Our study also takes advantage of MESA, which made robust analysis feasible given the availability of relevant databases for clinical and imaging confounders like cardiac MRI parameters and Agatston score.

The clinical value of these CT-based muscle measurements for various general medical diseases remains to be investigated. Deep learning algorithms (like ours employing semantic segmentation) are highly accurate methods of determining muscle measurements using CT, which has been robustly documented in the general literature (24,32,46). Additionally, previous studies have successfully implemented deep learning algorithms to measure imaging biomarkers and demonstrated predictive value in downstream events (47).

The ability to use IMAT and PAT indexes as predictors of incident HF cannot only improve HF prediction models but is also potentially useful in the monitoring of at-risk individuals. Detection of at-risk individuals can lead to higher clinical suspicion of HF. Early detection of HF in this context is critical to not only improve overall patient survival rate, but also to improve quality of life and slow the rate of disease progression (48).

Moreover, these indexes are potentially modifiable, unlike the nonmodifiable effects of predictors such as age and sex. As such, skeletal muscle loss may be a future target of secondary preventative measures (eg, nutritional and physical rehabilitation (16–18), leading to potentially

lower downstream risk of developing HF. For instance, aerobic exercises may have a protective effect on both skeletal and cardiac muscles (49). Additionally, in individuals who undergo consecutive CT examinations, interval changes in muscle and adipose measurements may be used to monitor the efficacy of these preventive measures.

Our study has several limitations. First, causal inference cannot be determined by our observational study. However, we attempted to address all available potential confounders in our studied association in a stepwise and thorough methodology, including all the available relevant data like imaging biomarkers (Agatston score and cardiac MRI). Second, the number of events for our longitudinal analysis was relatively small ($n = 41$). As such, extensive adjustment may contribute to overfitting of the final complete models. However, we have shown the association between the muscle and adipose parameters by showing both crude and fully adjusted models which show consistent trends. Moreover, MESA is one of the largest cohorts with robust clinical data and imaging available for such observational analysis. Third, our study used the most superior CT section including aortic arch as the landmark at which muscle parameters were extracted. Moreover, the aortic arch (used as our landmark for slice selection) typically increases in diameter and length with age (50). Additionally, arm position, respiratory phase, and conditions like kyphosis may affect slice quality. Consequently, the reliability of extracted muscle parameters from the eldest participants in the study may have been affected, though we attempted to standardize slice selection in a method similar to that in available literature (24). Fourth, our deep learning model was trained on an internal validation set due to data availability. External model validation is required to increase confidence in its reliability, though our model was trained, validated, and tested on CT scans from six different scanners, lending a degree of heterogeneity to the CT studies. Interobserver reliability of the CT-derived pectoralis muscle and adipose measurements was not formally assessed in this study. However, this exact methodology was manually implemented in a prior study on a similar cohort of patients to investigate longitudinal outcomes (24). Fifth, use of pectoralis muscle alone as opposed to or in conjunction with other muscle groups like paraspinal/abdominal muscles or volumetric analysis is also a limitation, as whole-body assessments could be more comprehensive. Still, the use of pectoralis muscle alone has been studied in literature as a validated predictor of health outcomes like mortality (eg, among individuals who underwent left ventricular device implantation) (24), (51,52). Sixth, the focus of our study was CT-based measurements as CT examinations may be more readily available because of their use as screening tools. However, cardiac MRI is another modality of choice to evaluate cardiac cachexia in individuals with known HF. As such, cardiac MRI may be a viable alternative imaging technique for pectoralis muscle and adipose measurements for prediction of events in individuals with established HF, such as all-cause mortality, hospitalization, and sudden cardiac death (44,45,53). Cardiac MRI may also provide information on additional markers such as epicardial fat (54) and lung water (55). Serial cardiac MRI measurements may also identify individuals with HF with ejection fraction recovery, who may have distinct HF outcomes (56). Finally, our study does not include intramyocellular lipids as an adiposity measure, as their detection and segmentation cannot be accurately performed using conventional CT. Other advanced imaging techniques like MRI spectroscopy are warranted for such analysis, which could be a subject for future investigations (57).

In conclusion, our study shows that deep learning derived pectoralis muscle and adipose area measurements can be reliably extracted from conventional chest CT. Although causal inference cannot be established in this observational study, higher intermuscular and perimuscular adipose area measurements were found to be associated with incident HF, demonstrating potential predictive value. As these measures may also be potentially modifiable (16–18), secondary preventive measures may be investigated for their ability to mitigate HF incidence in at-risk populations.

Acknowledgments: The authors thank the other investigators, the staff, and the participants of the MESA study for their valuable contributions. A full list of participating MESA investigators and institutions can be found at http://www.mesa-nhlbi.org. We would especially like to extend our acknowledgment to the MESA Lung for their valuable data on chest physiology.

Disclosures of conflicts of interest: Q.H. No relevant relationships. **H.A.I.** No relevant relationships. **D.A.B.** Former editor of *Radiology*. **F.P.** No relevant relationships. **A.K.** No relevant relationships. **J.G.K.** No relevant relationships. **R.C.** Speaker for Abbott Laboratories; spouse employed at Medtronic. **M.A.** No relevant relationships. **M.J.B.** NIH grant to institution. **R.G.B.** NIH grant to institution; COPD Foundation (unpaid scientific advisory role). **W.P.** NIH grant. **M.A.B.** No relevant relationships. **J.A.C.L.** No relevant relationships. **S.D.** Serves on the RSNA Publications Council and chairs the policy subcommittee.

References

1. Bowen RES, Graetz TJ, Emmert DA, Avidan MS. Statistics of heart failure and mechanical circulatory support in 2020. Ann Transl Med 2020;8(13):827.

2. Heidenreich PA, Fonarow GC, Opsha Y, et al. Economic Issues in Heart Failure in the United States. J Card Fail 2022;28(3):453–466.

3. Echouffo-Tcheugui JB, Butler J, Yancy CW, Fonarow GC. Association of Physical Activity or Fitness With Incident Heart Failure: A Systematic Review and Meta-Analysis. Circ Heart Fail 2015;8(5):853–861.

4. Tajik B, Voutilainen A, Sankaranarayanan R, et al. Frailty alone and interactively with obesity predicts heart failure: Kuopio Ischaemic Heart Disease Risk Factor Study. ESC Heart Fail 2023;10(4):2354–2361.

5. Kawel-Boehm N, Kronmal R, Eng J, et al. Left Ventricular Mass at MRI and Long-term Risk of Cardiovascular Events: The Multi-Ethnic Study of Atherosclerosis (MESA). Radiology 2019;293(1):107–114.

6. Wilson PWF, D'Agostino RB, Levy D, Belanger AM, Silbershatz H, Kannel WB. Prediction of coronary heart disease using risk factor categories. Circulation 1998;97(18):1837–1847.

7. Sahle BW, Owen AJ, Chin KL, Reid CM. Risk Prediction Models for Incident Heart Failure: A Systematic Review of Methodology and Model Performance. J Card Fail 2017;23(9):680–687.

8. Echouffo-Tcheugui JB, Greene SJ, Papadimitriou L, et al. Population risk prediction models for incident heart failure: a systematic review. Circ Heart Fail 2015;8(3):438–447.

9. Pocock SJ, Ariti CA, McMurray JJV, et al. Predicting survival in heart failure: a risk score based on 39 372 patients from 30 studies. Eur Heart J 2013;34(19):1404–1413.

10. Peterson PN, Rumsfeld JS, Liang L, et al. A validated risk score for in-hospital mortality in patients with heart failure from the American Heart Association get with the guidelines program. Circ Cardiovasc Qual Outcomes 2010;3(1):25–32.

11. Lee DS, Stitt A, Austin PC, et al. Prediction of heart failure mortality in emergent care: a cohort study. Ann Intern Med 2012;156(11):767–775, W-261, W-262.

12. Fonarow GC, Adams KF Jr, Abraham WT, Yancy CW, Boscardin WJ; ADHERE Scientific Advisory Committee, Study Group, and Investigators. Risk stratification for in-hospital mortality in acutely decompensated heart failure: classification and regression tree analysis. JAMA 2005;293(5):572–580.

13. Schnabel RB, Rienstra M, Sullivan LM, et al. Risk assessment for incident heart failure in individuals with atrial fibrillation. Eur J Heart Fail 2013;15(8):843–849.

14. Bakhshi H, Ambale-Venkatesh B, Yang X, et al. Progression of Coronary Artery Calcium and Incident Heart Failure: The Multi-Ethnic Study of Atherosclerosis. J Am Heart Assoc 2017;6(4):e005253.

15. Bluemke DA, Kronmal RA, Lima JAC, et al. The relationship of left ventricular mass and geometry to incident cardiovascular events: the MESA (Multi-Ethnic Study of Atherosclerosis) study. J Am Coll Cardiol 2008;52(25):2148–2155.

16. Okoshi MP, Capalbo RV, Romeiro FG, Okoshi K. Cardiac Cachexia: Perspectives for Prevention and Treatment. Arq Bras Cardiol 2017;108(1):74–80.

17. Horwich TB, Fonarow GC. Prevention of Heart Failure. JAMA Cardiol 2017;2(1):116.

18. Hersberger L, Dietz A, Bürgler H, et al. Individualized Nutritional Support for Hospitalized Patients With Chronic Heart Failure. J Am Coll Cardiol 2021;77(18):2307–2319.

19. Valentova M, Anker SD, von Haehling S. Cardiac Cachexia Revisited: The Role of Wasting in Heart Failure. Heart Fail Clin 2020;16(1):61–69.

20. Alahmad MAM, Acharya P, Morad A, Gupta K. Cardiac Cachexia Is Associated with a Prolonged Hospital Stay, Higher Mortality and No Increase Risk for 30-day Readmission after CHF Exacerbation. J Am Coll Cardiol 2022;79(9 Suppl):568.

21. Habaybeh D, de Moraes MB, Slee A, Avgerinou C. Nutritional interventions for heart failure patients who are malnourished or at risk of malnutrition or cachexia: a systematic review and meta-analysis. Heart Fail Rev 2021;26(5):1103–1118.

22. Huynh K, Ayers C, Butler J, et al. Association Between Thigh Muscle Fat Infiltration and Incident Heart Failure: The Health ABC Study. JACC Heart Fail 2022;10(7):485–493.

23. Mohajer B, Dolatshahi M, Moradi K, et al. Role of Thigh Muscle Changes in Knee Osteoarthritis Outcomes: Osteoarthritis Initiative Data. Radiology 2022;305(1):169–178.

24. Pishgar F, Shabani M, Quinaglia A C Silva T, et al. Quantitative Analysis of Adipose Depots by Using Chest CT and Associations with All-Cause Mortality in Chronic Obstructive Pulmonary Disease: Longitudinal Analysis from MESArthritis Ancillary Study. Radiology 2021;299(3):703–711.

25. Surov A, Kardas H, Besutti G, et al. Prognostic Role of the Pectoralis Musculature in Patients with COVID-19. A Multicenter Study. Acad Radiol 2023;30(1):77–82.

26. MESA Overview and Protocol. https://www.mesa-nhlbi.org/aboutMESAOverviewProtocol.aspx. Accessed September 8, 2023.

27. Carr JJ, Nelson JC, Wong ND, et al. Calcified coronary artery plaque measurement with cardiac CT in population-based studies: standardized protocol of Multi-Ethnic Study of Atherosclerosis (MESA) and Coronary Artery Risk Development in Young Adults (CARDIA) study. Radiology 2005;234(1):35–43.

28. Yaghoubi S, Tang W, Wang S, et al. Offline assessment of atherosclerotic coronary calcium from electron beam tomograms. Am J Card Imaging 1995;9(4):231–236.

29. Sieren JP, Newell JD Jr, Barr RG, et al. SPIROMICS Protocol for Multicenter Quantitative Computed Tomography to Phenotype the Lungs. Am J Respir Crit Care Med 2016;194(7):794–806.

30. GitHub - wkentaro/labelme: Image Polygonal Annotation with Python (polygon, rectangle, circle, line, point and image-level flag annotation). https://github.com/wkentaro/labelme. Accessed July 1, 2023.

31. Bradski G. (2000) The OpenCV Library. Dr. Dobb's Journal of Software Tools, 120; 122-125. - References - Scientific Research Publishing. https://www.scirp.org/(S(351jmbntvnsjt1aadkposzje))/reference/ReferencesPapers.aspx?ReferenceID=1692176. Accessed May 13, 2023.

32. Mühlberg A, Museyko O, Bousson V, Pottecher P, Laredo JD, Engelke K. Three-dimensional Distribution of Muscle and Adipose Tissue of the Thigh at CT: Association with Acute Hip Fracture. Radiology 2019;290(2):426–434.

33. Sheps SG. Overview of JNC VI: new directions in the management of hypertension and cardiovascular risk. Am J Hypertens 1999;12(8 Pt 2):65S–72S.

34. Expert Panel on Detection, Evaluation, and Treatment of High Blood Cholesterol in Adults. Executive Summary of The Third Report of The National Cholesterol Education Program (NCEP) Expert Panel on Detection, Evaluation, And Treatment of High Blood Cholesterol In Adults (Adult Treatment Panel III). JAMA 2001;285(19):2486–2497.

35. Schoenfeld D. Partial residuals for the proportional hazards regression model. Biometrika 1982;69(1):239–241.

36. Uno H, Cai T, Pencina MJ, D'Agostino RB, Wei LJ. On the C-statistics for evaluating overall adequacy of risk prediction procedures with censored survival data. Stat Med 2011;30(10):1105–1117.

37. Kent JT, O'quigley J. Measures of dependence for censored survival data. Biometrika 1988;75(3):525–534.

38. Moyer VA; U.S. Preventive Services Task Force. Screening for lung cancer: U.S. Preventive Services Task Force recommendation statement. Ann Intern Med 2014;160(5):330–338.

39. Latina J, Shabani M, Kapoor K, et al. Ultra-High-Resolution Coronary CT Angiography for Assessment of Patients with Severe Coronary Artery Calcification: Initial Experience. Radiol Cardiothorac Imaging 2021;3(4):e210053.

40. Shin JM, Kim TH, Kim JY, Park CH. Coronary artery calcium scoring on non-gated, non-contrast chest computed tomography (CT) using wide-detector, high-pitch and fast gantry rotation: comparison with dedicated calcium scoring CT. J Thorac Dis 2020;12(10):5783–5793.

41. Obisesan OH, Osei AD, Uddin SMI, Dzaye O, Blaha MJ. An Update on Coronary Artery Calcium Interpretation at Chest and Cardiac CT. Radiol Cardiothorac Imaging 2021;3(1):e200484.

42. Virani SS, Alonso A, Benjamin EJ, et al. Heart Disease and Stroke Statistics-2020 Update: A Report From the American Heart Association. Circulation 2020;141(9):e139–e596.

43. Contaldi C, Dellegrottaglie S, Mauro C, et al. Role of Cardiac Magnetic Resonance Imaging in Heart Failure. Heart Fail Clin 2021;17(2):207–221.

44. Cunha GJL, Rocha BML, Freitas P, et al. Pectoralis major muscle quantification by cardiac MRI is a strong predictor of major events in HF. Heart Vessels 2022;37(6):976–985.

45. Kumar A, Ansari BA, Kim J, et al. Axial Muscle Size as a Strong Predictor of Death in Subjects With and Without Heart Failure. J Am Heart Assoc 2019;8(4):e010554.

46. Youn S, Jogiat U, Baracos VE, McCall M, Eurich DT, Sawyer MB. CT-based assessment of body composition and skeletal muscle in melanoma: A systematic review. Clin Nutr ESPEN 2021;45:127–133.

47. Mohajer B, Moradi K, Guermazi A, et al. Diabetes-associated thigh muscle degeneration mediates knee osteoarthritis-related outcomes: results from a longitudinal cohort study. Eur Radiol 2023;33(1):595–605.

48. de Couto G, Ouzounian M, Liu PP. Early detection of myocardial dysfunction and heart failure. Nat Rev Cardiol 2010;7(6):334–344.

49. Giannuzzi P, Temporelli PL, Corrà U, Tavazzi L; ELVD-CHF Study Group. Antiremodeling effect of long-term exercise training in patients with stable chronic heart failure: results of the Exercise in Left Ventricular Dysfunction and Chronic Heart Failure (ELVD-CHF) Trial. Circulation 2003;108(5):554–559.

50. Hickson SS, Butlin M, Graves M, et al. The relationship of age with regional aortic stiffness and diameter. JACC Cardiovasc Imaging 2010;3(12):1247–1255.

51. Bak SH, Kwon SO, Han SS, Kim WJ. Computed tomography-derived area and density of pectoralis muscle associated disease severity and longitudinal changes in chronic obstructive pulmonary disease: a case control study. Respir Res 2019;20(1):226.

52. Teigen LM, John R, Kuchnia AJ, et al. Preoperative pectoralis muscle quantity and attenuation by computed tomography are novel and powerful predictors of mortality after left ventricular assist device implantation. Circ Heart Fail 2017;10(9):e004069.

53. Manolis AS, Manolis AA, Manolis TA, Melita H. Sudden death in heart failure with preserved ejection fraction and beyond: an elusive target. Heart Fail Rev 2019;24(6):847–866.

54. Cheang I, Zhu X, Yue X, et al. Prognostic value of ventricle epicardial fat volume by cardiovascular magnetic resonance in chronic heart failure. iScience 2023;26(5):106755.

55. Rocha BML, Cunha GJL, Freitas P, et al. Measuring lung water adds prognostic value in heart failure patients undergoing cardiac magnetic resonance. Sci Rep 2021;11(1):20162.

56. Lupón J, Díez-López C, de Antonio M, et al. Recovered heart failure with reduced ejection fraction and outcomes: a prospective study. Eur J Heart Fail 2017;19(12):1615–1623.

57. Kim HK, Serai S, Lindquist D, et al. Quantitative Skeletal Muscle MRI: Part 2, MR Spectroscopy and T2 Relaxation Time Mapping-Comparison Between Boys With Duchenne Muscular Dystrophy and Healthy Boys. AJR Am J Roentgenol 2015;205(2):W216–W223.

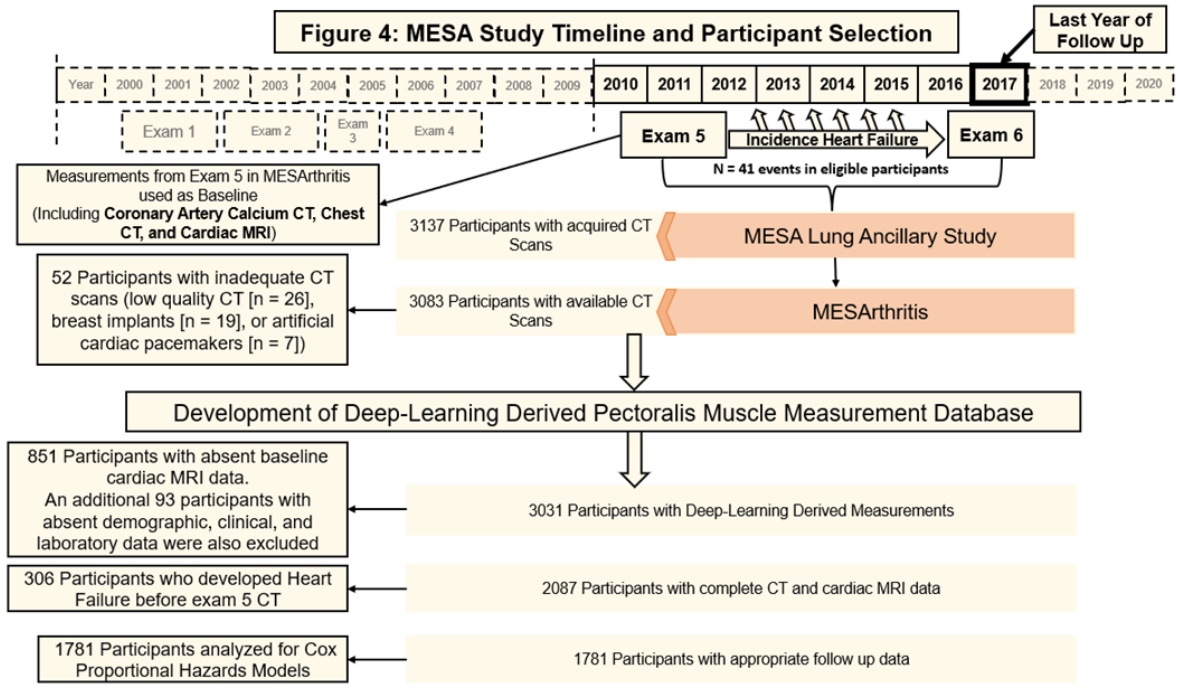

Figure 1: MESA study timeline and participant selection. MESA = Multi-Ethnic Study of Atherosclerosis.

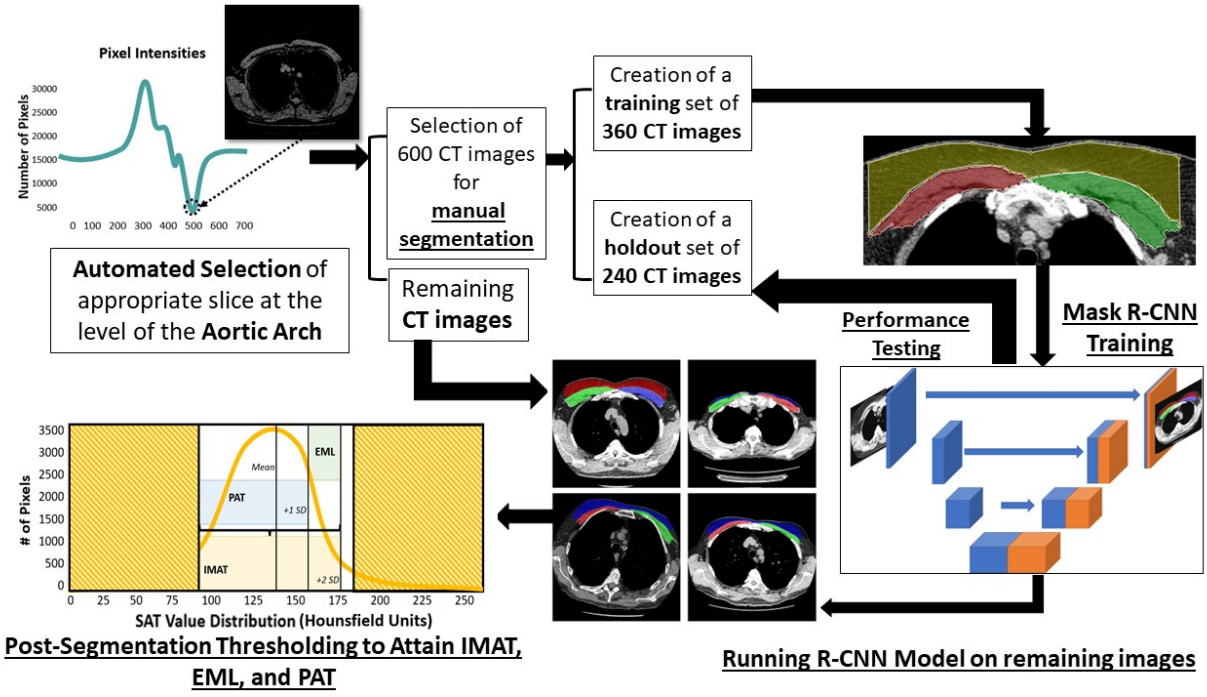

Figure 2: Workflow of deep learning algorithm development. SAT = Subcutaneous Adipose Tissue, IMAT = Intermuscular Adipose Tissue, PAT = Perimuscular Adipose Tissue, EML = Extramyocellular Lipid, *R*-CNN = region-based convolutional neural network.

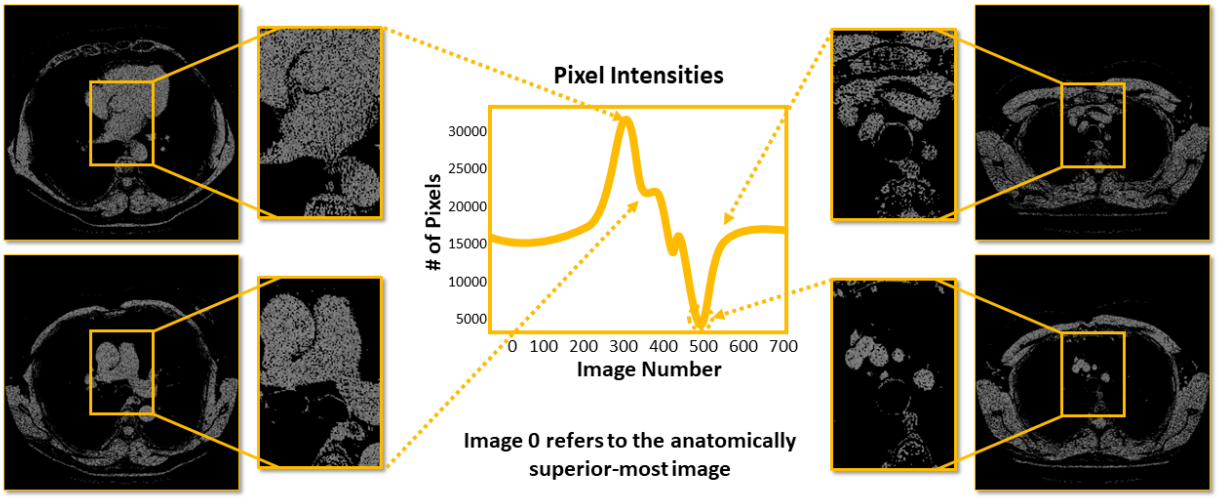

Figure 3: Automatic selection of slice above the aortic arch using analysis of pixel intensities.

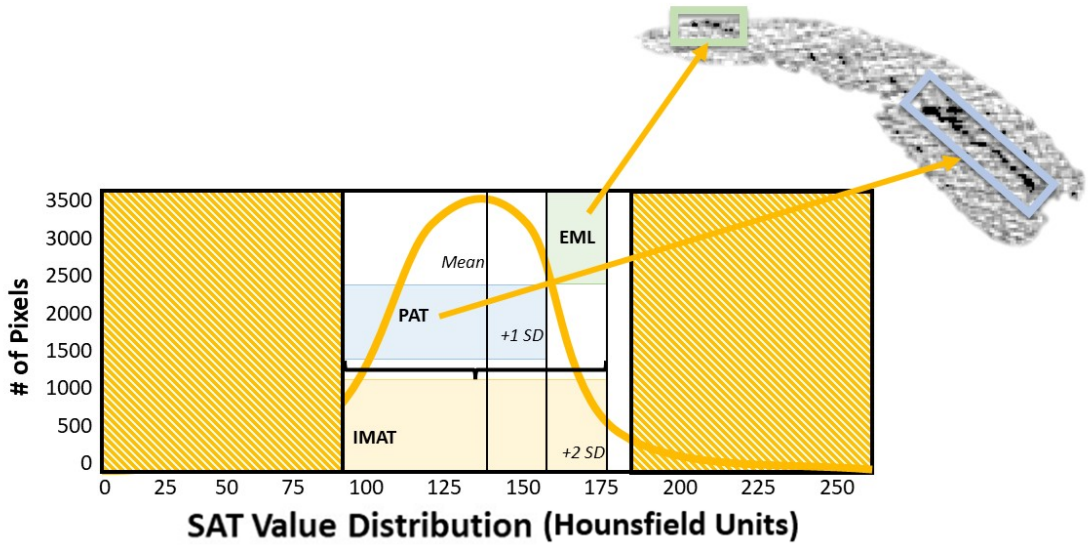

Figure 4: Visualization of individualized thresholding framework to identify intermuscular adipose tissue and its subcomponents. SAT = Subcutaneous Adipose Tissue, IMAT = Intermuscular Adipose Tissue, PAT = Perimuscular Adipose Tissue, EML = Extramyocellular Lipid. The cross-hatched sections represent trimmed values from the upper and lower distribution chart.

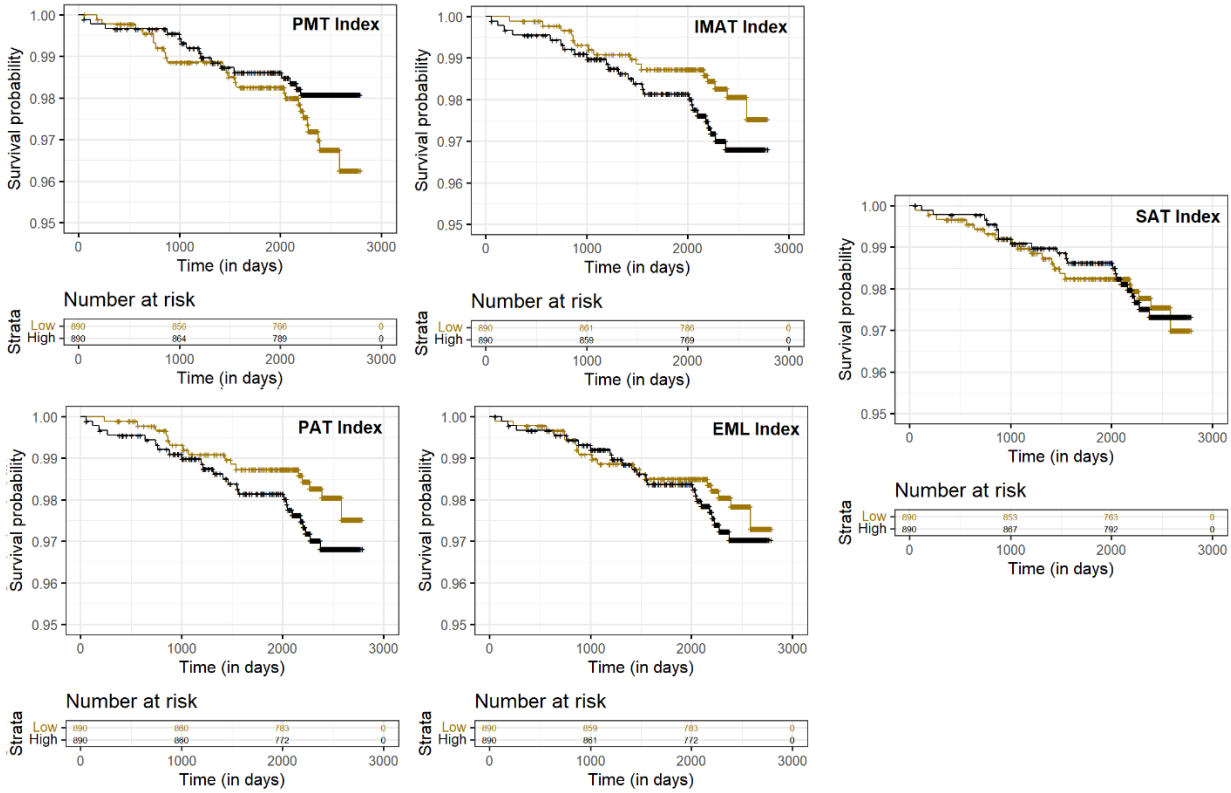

Figure 5: Kaplan-Meier estimates of incident heart failure using muscle indexes, categorized by median values. The x-axis shows time (in days), and the y-axis shows the survival probability. The following indexes were studied: Intermuscular Adipose Tissue (IMAT, Median: 1.2 cm^2/m^2), Extramyocellular Lipid, (EML, Median: 0.4 cm^2/m^2), Perimuscular Adipose Tissue (PAT, Median: 0.8 cm^2/m^2), Pectoralis Muscle Tissue (PMT, Median: 11.6 cm^2/m^2), and Subcutaneous Adipose Tissue (SAT, Median: 12.4 cm^2/m^2). Lower than median curves are shown in yellow. Higher than median curves are shown in black.

Table 1

Baseline Descriptive Statistics of MESA Participants without Heart Failure

Characteristic	*n* = 1,781[1]
Age (y)	68 (61, 75)
Sex	

Female	907 (51%)
Male	874 (49%)
Race/Ethnicity	
Black	463 (26%)
White/Caucasian	696 (39%)
Other	622 (35%)
Total Gross Family Income	
≤$5,000	20 (1.1%)
$5,000-$24,999	314 (18%)
$24,999–49,999	616 (35%)
≥$50,000	831 (47%)
Body Mass Index (kg/m^2)	27.5 (24.4, 30.9)
Pack Years of Smoking	0.0 (0.0, 13.5)
Presently Drink Alcohol	
No	1,013 (57%)
Yes	768 (43%)
Moderate to Vigorous Activity (MET-min/week)	3,577.5 (1,672.5, 7,012.5)
Left Ventricular Ejection Fraction (%)	69.1 (65.1, 72.8)
Hemoglobin A1C (%)	5.7 (5.5, 6.1)
Serum Creatinine (mg/dL)	0.9 (0.7, 1.0)
Hypertension	
No	834 (47%)
Yes	947 (53%)
Total Cholesterol	
<200 mg/dL	1,208 (68%)
≥200 mg/dL	573 (32%)
Hypertension Medication Use	
No	834 (47%)
Yes	947 (53%)
Lipid-lowering Medication Use	
No	1,124 (63%)
Yes	657 (37%)
Insulin/Hypoglycemic Medication Use	
No	1,528 (86%)
Yes	253 (14%)
Phantom-adjusted Total Agatston Calcium Score	32.03 (0.00, 225.70)
Intermuscular Adipose Tissue Index 1 (Intermuscular Adipose Tissue Area by Height Squared (cm^2/m^2)	1.18 (0.58, 2.28)
Extramyocellular Adipose Tissue Index 1 (Extramyocellular Adipose Tissue Area by Height Squared (cm^2/m^2)	0.37 (0.20, 0.70)
Perimuscular Adipose Tissue Index 1 (Perimuscular Adipose Tissue Area by Height Squared (cm^2/m^2)	0.79 (0.37, 1.58)
Pectoralis Muscle Index (Pectoralis Muscles Area by Height Squared (cm^2/m^2)	11.60 (8.99, 14.59)
Subcutaneous Adipose Tissue Index (Subcutaneous Adipose Tissue Area by height Squared (cm^2/m^2)	12.35 (7.24, 21.17)

Note.—MESA = Multi-Ethnic Study of Atherosclerosis.

[1] Median (IQR); *n* (%).

Table 2

Intersection Over Union and Dice Similarity Coefficients of the Deep Learning Model

	Intersection Over Union (95% CI)	Dice Similarity Coefficient (95% CI)
Overall	0.82 (0.82, 0.83)	0.90 (0.90, 0.91)
Left Pectoralis Muscle Masks	0.79 (0.78, 0.80)	0.88 (0.87, 0.89)
Right Pectoralis Muscle Masks	0.79 (0.78, 0. 80)	0.88 (0.87, 0.89)
Subcutaneous Adipose Tissue Masks	0.75 (0.74, 0.76)	0.85 (0.84, 0.86)

Table 3

Cox-proportional Hazard Models Using Pectoralis Muscle and Adipose Indices to Predict Incident Heart Failure

	Crude Models[1]		Full Imaging (Coronary Artery Calcium Score + Cardiac MRI)[2]	
Muscle Parameter	Hazard Ratio (95% CI)	*P* value	Hazard Ratio (95% CI)	*P* value
Pectoralis Muscle Index[3]	0.98 [0.92, 1.04]	0.48	0.98 [0.91, 1.05]	0.57
Intermuscular Adipose Index[4]	1.14 [1.03, 1.26]	0.01	1.16 [1.03, 1.31]	0.02
Extramyocellular Adipose Index[5]	1.45 [0.97, 2.16]	0.07	1.37 [0.89, 2.13]	0.16
Perimuscular Adipose Area Index[6]	1.19 [1.06, 1.35]	0.01	1.25 [1.07, 1.46]	0.01
Subcutaneous Adipose Index[7]	1.00 [0.97, 1.03]	0.83	1.02 [0.98, 1.06]	0.29

[1] Unadjusted Models.

[2] Adjusted for Age, Race, Sex, Moderate to Vigorous Physical Activity (MET-min/week), log (Phantom Adjusted Total Agatston Calcium Score), Left Ventricular Ejection Fraction, Left Ventricular Mass Percentage of Predicted, Total Gross Family Income, Pack Years of Smoking, Present Alcohol Consumption, Hypertension, Total Cholesterol (NCEP Guidelines), Hemoglobin A1C (%), Hypertension Medication Use, Insulin/Hypoglycemic Medication Use, Lipid-lowering Medication use, and Creatinine (mg/dL).

[3] Pectoralis Muscle Area (cm^2) by Height (m^2).

[4] Intermuscular Adipose Area (cm^2) by Height (m^2).

[5] Extramyocellular Adipose Area (cm^2) by Height (m^2).

[6] Perimuscular Adipose Area (cm^2) by Height (m^2).

[7] Subcutaneous Adipose Area (cm^2).

Appendix–Supplementary Text

Figure E1 provides a visual comparison between inferences drawn by the deep-learning algorithm and a schematic representation of the different adipose distributions. These were shown using the same example frame selected directly superior to the aortic arch.

Figure E2 highlights the process of region of interest creation for the subcutaneous adipose tissue, right pectoralis muscle, and left pectoralis muscles.

Figure E3 highlights the segmentations acquired by the deep-learning algorithm across different patients, showcasing the performance of our algorithm in nonideal conditions. The algorithm begins by removing abdominal frames and selecting the slice above the aortic arch based on mediastinal pixel intensities before automated segmentation of the pectoralis muscle groups and the subcutaneous adipose tissue. The colors of the masks vary across acquisitions but were correctly assigned to the appropriate anatomic segments.

To help determine the discrimination and goodness-of-fit of the various models presented in this article, we calculated the Harrell's C-statistic and Kent and O'Quigley Pseudo-R^2 metrics for each set of Cox-Proportional Hazards Models (Table E1).

To increase clinical interpretability of our results, we also reconstructed our initial analyses using metrics of raw area measurements (cm^2) in lieu of indexed measurements (Table E2).

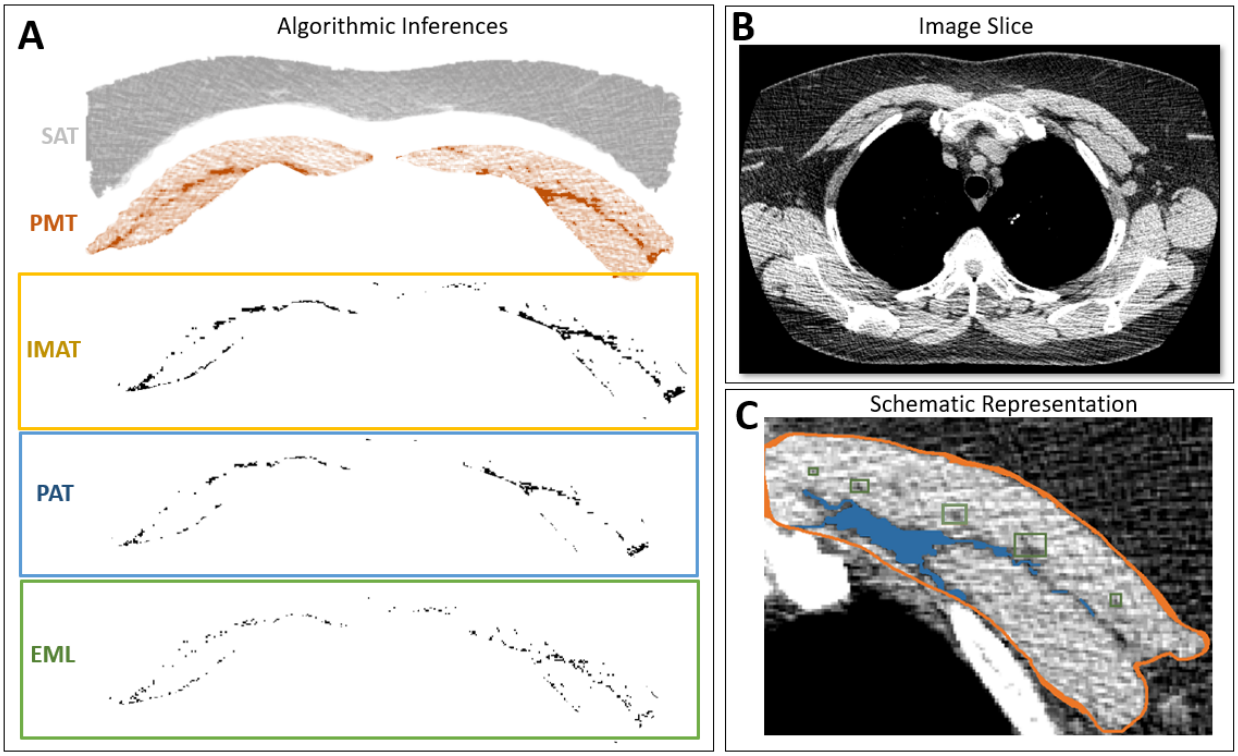

Figure E1: **(A)** Inferences of Pectoralis Muscle Area Measurements using the Deep-Learning Algorithm and Quantitative Assessment Framework. **(B)** Sample Image Slice. **(C)** Schematic Representation of Muscle Area (Orange), Extramyocellular Lipids (Green) and Perimuscular Adipose Tissue (Blue). SAT = Subcutaneous Adipose Tissue, PMT = Pectoralis Muscle Tissue, IMAT = Intermuscular Adipose Tissue, PAT = Perimuscular Adipose Tissue, EML = Extramyocellular Lipid.

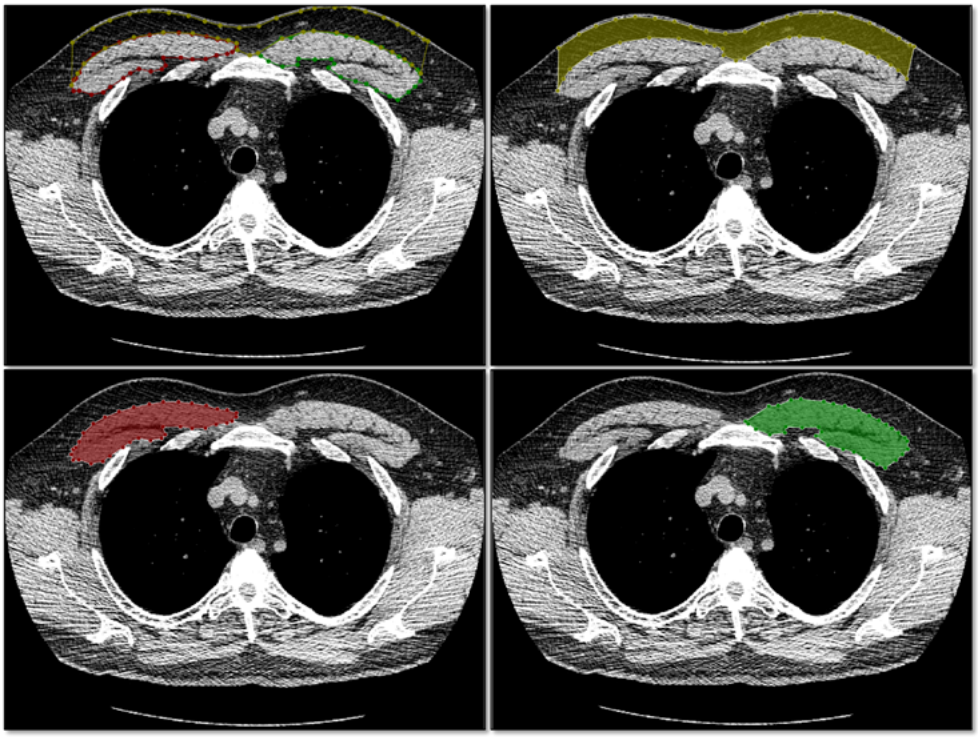

Figure E2: Example regions of interest for subcutaneous adipose tissue (yellow), right pectoralis muscle (red), and left pectoralis muscle (green).

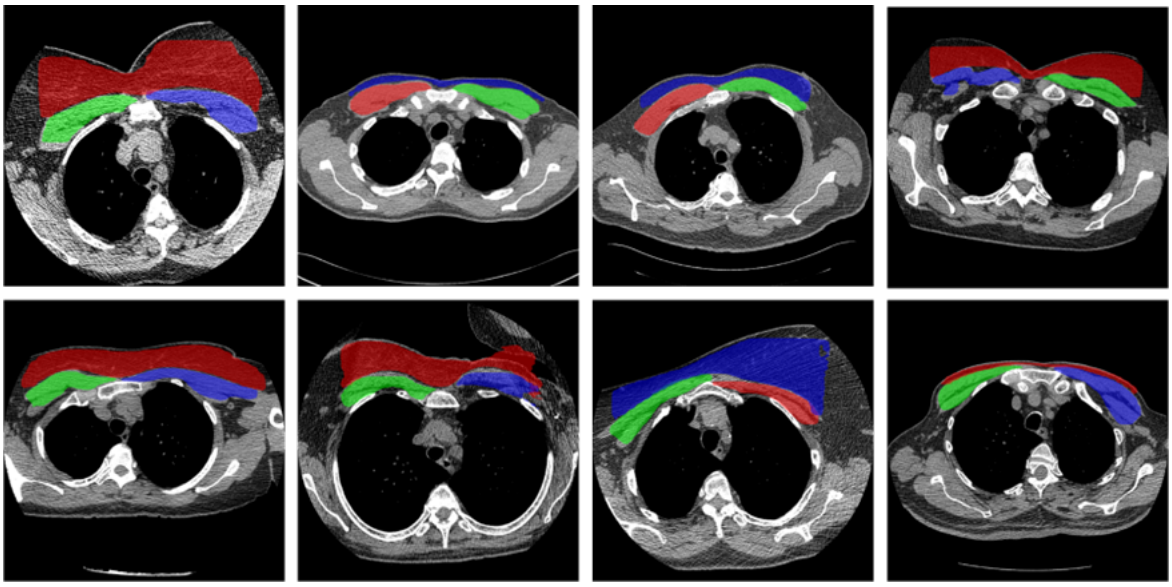

Figure E3: Example segmentations derived using the automated deep-learning segmentation platform across from different patients. The algorithm begins by removing abdominal frames and selecting the slice above the aortic arch based on mediastinal

pixel intensities before automated segmentation of the pectoralis muscle groups and the subcutaneous adipose tissue. The colors of the masks vary across acquisitions but were correctly assigned to the appropriate anatomic segments.

Table E1

Harrell's C-statistic and Kent and O'Quigley Pseudo R^2 of Cox-proportional Hazard Models Using Pectoralis Muscle and Adipose Indices to Predict Incident Heart Failure

	Crude Models[1]		Full Imaging (Coronary Artery Calcium Score + Cardiac MRI)[2]	
Muscle Parameter	Harrell's C-statistic (95% Confidence Interval)	Kent and O'Quigley Pseudo R^2	Harrell's C-statistic (95% Confidence Interval)	Kent and O'Quigley Pseudo R^2
Pectoralis Muscle Index[3]	0.54 [0.47, 0.61]	0.007	0.85 [0.79, 0.90]	0.482
Intermuscular Adipose Index[4]	0.57 [0.47, 0.67]	0.038	0.85 [0.79, 0.91]	0.499
Extramyocellular Adipose Index[5]	0.54 [0.44, 0.64]	0.027	0.85 [0.79, 0.90]	0.489
Perimuscular Adipose Area Index[6]	0.57 [0.47, 0.67]	0.035	0.85 [0.79, 0.81]	0.504
Subcutaneous Adipose Index[7]	0.49 [0.41, 0.57]	0.001	0.85 [0.71, 0.81]	0.487

[1] Unadjusted Models.

[2] Adjusted for Age, Race, Sex, Moderate to Vigorous Physical Activity (MET-min/week), log (Phantom Adjusted Total Agatston Calcium Score), Left Ventricular Ejection Fraction, Left Ventricular Mass Percentage of Predicted, Total Gross Family Income, Pack Years of Smoking, Present Alcohol Consumption, Hypertension, Total Cholesterol (NCEP Guidelines), Hemoglobin A1C (%), Hypertension Medication Use, Insulin/Hypoglycemic Medication Use, Lipid-lowering Medication use, and Creatinine (mg/dL).

[3] Pectoralis Muscle Area (cm^2) by Height (m^2).

[4] Intermuscular Adipose Area (cm^2) by Height (m^2).

[5] Extramyocellular Adipose Area (cm^2) by Height (m^2).

[6] Perimuscular Adipose Area (cm^2) by Height (m^2).

[7] Subcutaneous Adipose Area (cm^2).

Table E2

Cox-proportional Hazard Models Using Raw Pectoralis Muscle and Adipose Areas to Predict Incident Heart Failure

	Crude Models[1]		Full Imaging (Coronary Artery Calcium Score + Cardiac MRI)[2]	
Muscle Parameter	Hazard Ratio (95% Confidence Interval)	*P* value	Hazard Ratio (95% CI)	*P* value
Pectoralis Muscle Index[3]	0.99 [0.97, 1.01]	0.49	0.99 [0.96, 1.02]	0.57
Intermuscular Adipose Index[4]	1.05 [1.01, 1.09]	0.02	1.05 [1.01, 1.11]	0.03
Extramyocellular Adipose Index[5]	1.15 [0.99, 1.34]	0.07	1.13 [0.95, 1.34]	0.17
Perimuscular Adipose Area Index[6]	1.06 [1.02, 1.11]	0.001	1.08 [1.02, 1.15]	0.01
Subcutaneous Adipose Index[7]	0.99 [0.99, 1.01]	0.87	1.01 [0.99, 1.03]	0.25

[1] Unadjusted Models.

[2] Adjusted for Age, Race, Sex, Moderate to Vigorous Physical Activity (MET-min/week), log (Phantom Adjusted Total Agatston Calcium Score), Left Ventricular Ejection Fraction, Left Ventricular Mass Percentage of Predicted, Total Gross Family Income, Pack Years of Smoking, Present Alcohol Consumption, Hypertension, Total Cholesterol (NCEP Guidelines), Hemoglobin A1C (%), Hypertension Medication Use, Insulin/Hypoglycemic Medication Use, Lipid-lowering Medication use, and Creatinine (mg/dL).

[3] Pectoralis Muscle Area (cm^2) by Height (m^2).

[4] Intermuscular Adipose Area (cm^2) by Height (m^2).

[5] Extramyocellular Adipose Area (cm^2) by Height (m^2).

[6] Perimuscular Adipose Area (cm^2) by Height (m^2).

[7] Subcutaneous Adipose Area (cm^2).

RSNA

Predictive Value of Deep Learning-derived CT Pectoralis Muscle and Adipose Measurements for Incident Heart Failure: Multi-Ethnic Study of Atherosclerosis

Key Result
The deep learning algorithm produced reliable CT-based pectoralis muscle and adipose area measurements, which may be predictive of incident heart failure.

Participants:
- 1,781 participants (median age, 68 [IQR, 61-75] years) without baseline heart failure (from MESA study)

Methods:
- A deep learning algorithm for pectoralis muscle and adipose area measurements was developed using individualized thresholds from chest CT examinations.
- Longitudinal association between baseline measurements and incident heart failure using stepwise Cox proportional hazards models.

Results:
- The model achieved a Dice score of 0.90 on both the training and testing sets.
- In models fully adjusted for clinical and imaging confounders, intermuscular adipose tissue (*IMAT*, HR: 1.16; 95% CI: 1.03, 1.31) and perimuscular adipose tissue (*PAT*, HR: 1.25; 95% CI: 1.07, 1.46) predicted incident heart failure.

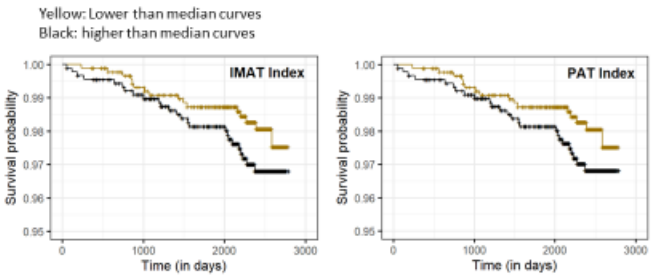

Hathaway and Ibad et al. Published Online: October 5, 2023
https://doi.org/10.1148/ryct.230146
Radiology: Cardiothoracic Imaging